Biomaterials xxx (2013) 1–11

Contents lists available at SciVerse ScienceDirect

Biomaterials

journal homepage: www.elsevier.com/locate/biomaterials

[^{123}I]Iodooctyl fenbufen amide as a SPECT tracer for imaging tumors that over-express COX enzymes

Ho-Lien Huang [a,1], Chun-Nan Yeh [b,1], Wei-Yuan Lee [a], Ying-Cheng Huang [c], Kang-Wei Chang [d], Kun-Ju Lin [e], Shu-Fan Tien [a], Wen-Chin Su [a,d], Ching-Hsiuan Yang [d], Jenn-Tzong Chen [d], Wuu-Jyh Lin [d], Shio-Shio Fan [d], Chung-Shan Yu [a,f,*]

[a] Department of Biomedical Engineering and Environmental Sciences, National Tsing-Hua University, Hsinchu 300, Taiwan
[b] Department of Surgery, Chang Gung Memorial Hospital at Linkou, Chang Gung University, Taiwan
[c] Department of Neurosurgery, Chang Gung Memorial Hospital at Linkou, Chang Gung University, Taiwan
[d] Institute of Nuclear Energy Research, Taoyuan 32546, Taiwan
[e] Department of Nuclear Medicine, Chang Gung Memorial Hospital at Linkou, Chang Gung University, Taiwan
[f] Institute of Nuclear Engineering and Science, National Tsing-Hua University, Hsinchu 300, Taiwan

ARTICLE INFO

Article history:
Received 17 December 2012
Accepted 9 January 2013
Available online xxx

Keywords:
Imaging
Tumor
Radiochemistry
Nuclear medicine
Inflammation

ABSTRACT

This study is concerned with the development of an agent for single photon emission computer tomography (SPECT) for imaging inflammation and tumor progression. [^{123}I]Iodooctyl fenbufen amide ([^{123}I]IOFA) was prepared from the precursor *N*-octyl-4-oxo-4-(4′-(trimethylstannyl)biphenyl-4-yl) butanamide with a radiochemical yield of 15%, specific activity of 37 GBq/μmol, and radiochemical purity of 95%. Analysis of the binding of [^{123}I]IOFA to COX-1 and COX-2 enzymes by using HPLC and a gel filtration column showed a selectivity ratio of 1:1.3. An assay for the competitive inhibition of substrate transfer showed that IOFA exhibited a comparable IC_{50} value compared to fenbufen. In the normal rat liver, a lower level and homogeneous pattern of [^{123}I]IOFA radioactivity was observed by SPECT. In contrast, in the rat liver with thioacetamide-induced cholangiocarcinoma, a higher uptake and heterogeneous pattern of [^{123}I]IOFA radioactivity was seen as hot spots in tumor lesions by SPECT imaging. Importantly, elevated COX-1 and COX-2 expressions from immunostaining were found in the bile ducts of tumor rats but not of normal rats. Therefore, [^{123}I]IOFA was found to exhibit the potential for imaging tumors that over-express COX.

1. Introduction

Non-steroid anti-inflammatory drugs (NSAIDs) have been well recognized for their anti-inflammatory efficacy and cancer-preventing effects. Chronic inflammation is associated with an increased risk of cancer for individuals with inflammatory bowel diseases [1]. Hence, cancer prevention by using NSAIDs is a relevant concept, and reports on their use for this means can be found in literature [2,3]. Their inflammatory mechanism is mainly associated with inflammatory lipids that are catalyzed by the key enzyme, cyclooxygenase (COX) [4]. Three types of COX enzymes have been reported: (1) COX-1, which functions as a house-keeping enzyme and is constitutively expressed in most tissue types; (2) COX-2, which is a highly inducible enzyme under physiological conditions; and (3) a COX-1 splice variant that is termed COX-3 [5–7]. COX mediates the conversion of arachidonic acid (AA) into prostaglandins (PG) via two sequential steps: initial oxidation to PGG2 by using a cyclooxygenase enzyme and subsequent reduction to an unstable endoperoxide intermediate PGH2 by peroxidase (POX) [8]. The two reactions occur in spatially distinct but mechanistically coupled active sites. The cyclooxygenase active site is located at the end of a long hydrophobic channel that is broad near the membrane-binding domain (the lobby) and narrows as it extends toward the interior of the protein [9,10]. The POX active site is located on the surface of the protein near the heme cofactor. Prostaglandin endoperoxide synthase-1 and -2 (PGHS-1 and -2) are also known as COX-1 and COX-2, respectively [11]. PGHSs are composed of two monomers. Each monomer has a physically distinct COX and POX active site. The two monomers have different conformations, and they function cooperatively during catalysis in solution. It is clear

* Corresponding author. Department of Biomedical Engineering and Environmental Sciences, National Tsing-Hua University, Hsinchu 300, Taiwan.
E-mail address: csyu@mx.nthu.edu.tw (C.-S. Yu).
[1] These authors made equal contributions to this study.

0142-9612/$ – see front matter © 2013 Elsevier Ltd. All rights reserved.
http://dx.doi.org/10.1016/j.biomaterials.2013.01.050

that the COX reaction is activated through a radical cation intermediate of a heme–monomer complex that is derived from the oxidation of the heme–monomer complex by POX. The key rests in the fact that the Tyr^{385} radical should be formed via POX before the oxidation of AA by COX. COX and POX could maintain their reaction pathways independently. However, the reaction cycle of COX is sensitive and could be terminated by various factors, whereas POX activity is relatively unaffected and can last longer.

The mechanism of inhibition of COXs by traditional NSAIDs is complicated because AA and the inhibitor interact with COX reciprocally. In PGHS-1, the conformations of the two AAs in the AA-COX complexes of the dimer are symmetrical. In contrast, the two conformations of AAs in PGHS-2 are antisymmetrical [12]. PGHS-2 functions as a conformational heterodimer with an allosteric monomer (E_{allo}) and a catalytic (E_{cat}) monomer. For example, some non-substrate fatty acids could bind E_{allo} to stimulate the rate of AA oxygenation. Some COX inhibitory NSAIDs and some COX-2 specific inhibitors function through E_{allo}, E_{cat}, or both E_{allo} and E_{cat} [13,14]. In many tumors, high prostaglandin levels are up-regulated by COX, whereas the degraded enzyme e.g., 15-prostagladin dehydrogenase (15-PGDH) plays a role in the negative regulation of prostaglandin levels.

The long-term uptake of NSAIDs and COX-1inhibitors is always accompanied by adverse side effects such as gastrointestinal toxicity [15,16]. Specific COX-2 inhibitors were developed to overcome this side effect. However, prolonged use of COX-2 inhibitors results in other side effects such as cardiovascular events. Furthermore, very high dosages of COX inhibitors or NSAIDs are frequently required to exhibit tumor inhibition effects, but only low dosages are required for inhibiting prostaglandin formation [1,17]. The antitumoral effects are thus probably not only mediated through the COX pathway but also through an NSAID-activated gene or growth differentiation factor 15 [1].

Because of the complexity of COX mechanisms such as dual functionality of the enzyme and close coupling of the two active sites, agents with unique inhibitory properties are still under development. Apart from the fact that aspirin irreversibly inactivates COX-2 by covalently modifying E_{cat}, other COX inhibitors have been developed such as (a) time-independent E_{allo} inhibitors (ibuprofen with 2-arachidonylglycerol and PGHS-2) or time-independent E_{allo} and E_{cat} inhibitors (ibuprofen with AA and PGHS-2), and (b) time-dependent E_{allo} inhibitors (naproxen with AA and PGHS-2) [11,13,14]. In addition, a number of studies have focused on developing COX-1 selective inhibitors with very low gastric ulcerogenic activities [18,19], because inhibiting COX-1 alone is not sufficient to cause gastric damage [20].

Imaging inflammation as well as tumor progression has attracted a great deal of attention recently [21–36]. As a diagnostic imaging probe for positron emission tomography (PET) or single photon emission computer tomography (SPECT), cytotoxicity is not a serious concern because only very low doses (lower than 1/100 the therapeutic dose) are administered to an individual within a short period [37]. Various PET and SPECT probes based on the structural characteristics of COX-2 [21–35] and COX-1 [36] specific inhibitors have been developed in the past few decades. However, only rare radiopharmaceuticals have been successfully applied to imaging inflammatory events [36]. The reason for this has been attributed to the instability of COX-2 enzymes or due to the very low absolute amount of COX-2 over-expression that is available to be detected [1].

Because the designs of these radiolabeled COX-2 inhibitors are mainly based on a triphenyl ring scaffold or biaryl scaffold that specifically target the COX-2 enzyme, other types of radiopharmaceuticals that target the COX-1 enzyme have been re-investigated [38]. Promising imaging results [39] encouraged us to prepare octyl fenbufen amide (OFA) [40–42], which are members of the NSAID family that do not exhibit COX selectivity (Fig. 1). Specifically, OFA was discovered through parallel solution phase synthesis. Moreover, the octyl group can be used to modify its antitumoral cytotoxicity ($EC_{50} = 20$ μM) in comparison with its parent fenbufen [42]. Arachidonyl ethanolamide (AEA) was reported to be poly-unsaturated fatty acyl amide that exerts immunomodulatory activity through unspecified anchoring to the active site of COX-2 (as well as COX-1) [43,44]. Because both AEA and OFA share a similar structural feature in terms of their eight-carbon chain length, the inhibition of cellular growth by OFA was postulated to be mediated through such an interaction. Hence, OFA might be a tracer suitable for imaging COX function. Taken together, OFA was chosen for radiolabeling and for imaging of COXs in vivo. Specifically, OFA was labeled with radioiodine ^{123}I for non-invasive in vivo imaging using SPECT.

2. Materials and methods

2.1. General

All of the reagents and solvents that we used were purchased from Sigma–Aldrich, Malingkrodt, Acros, Alfa, Tedia, or Fluka. CH_2Cl_2 and toluene were dried over CaH_2, and MeOH was dried over Mg and distilled prior to use. DMF and 1,4-dioxane were distilled under reduced pressure. The reagents and solvents were reagent grade. Preparation of organostannyl compound **3** was carried out in dried glassware under nitrogen at positive pressure. The eluents that were used for flash chromatography such as EtOAc, acetone, and *n*-hexane were of industrial grade and distilled prior to use; MeOH and $CHCl_3$ were reagent grade and used without further purification. Thin layer chromatography (TLC) was performed with MERCK TLC silica gel 60 F_{254} precoated plates. The starting materials and products were visualized with UV light (254 nm). Further confirmation was carried out by staining with 5% *p*-anisaldehyde, ninhydrin, or ceric ammonium molybdate under heating. Flash chromatography was performed using Geduran Si 60 silica gel (230–400 mesh). Melting points were measured with MEL-TEMP and were uncorrected. NMR spectroscopy, including ^1H NMR (500 MHz) and ^{13}C NMR (125 MHz, DEPT-135), was performed on a Varian Unity Inova 500 MHz. D-solvents that were employed for NMR, including CD_3OD, $CDCl_3$, and C_6D_6, were purchased from Cambridge Isotope Laboratories, Inc. Low-Resolution Mass Spectrometry (LRMS) was performed on an ESI-MS spectrometer by employing a VARIAN 901-MS Liquid Chromatography Tandem Mass Q-Tof Spectrometer at the Department of Chemistry of National Tsing-Hua University (NTHU). High Resolution Mass Spectrometry (HRMS) was performed using a varian HPLC (prostar series ESI/APCI) coupled mass detector from a Varian 901-MS (FT-ICR Mass) and a triple quadrapole.

A commercial colorimetric COX (ovine) inhibitor screening assay kit was purchased from Cayman Chemical Ltd (760111). The assay kit contained both COX-1 and

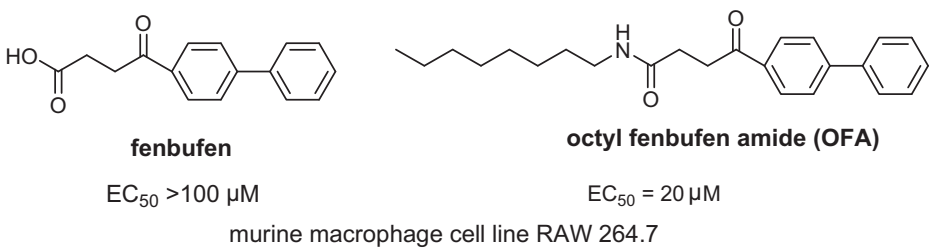

Fig. 1. Enhanced inhibition of cellular growth by octyl fenbufen amide.

Please cite this article in press as: Huang H-L, et al., [^{123}I]Iodooctyl fenbufen amide as a SPECT tracer for imaging tumors that over-express COX enzymes, Biomaterials (2013), http://dx.doi.org/10.1016/j.biomaterials.2013.01.050

COX-2 assay reagents. The specific activities of both the two enzymes were equivalent according to the suppliers. A commercial PTFE filter (0.45 μm) was purchased from Millipore. An Elisa reader of 96 well (Biochrom, Anthos Zenyth 3100) was set at $\lambda_{max} = 595$ nm according to the kit supplier. The IC_{50} calculation was made by using commercial software of Graph Pads.

[^{123}I]NaI was produced on an EBCO TR30 cyclotron (30 MeV) via the ^{124}Xe(p,2n)^{123}Cs → ^{123}Xe → ^{123}I at Nuclear Energy Research Institute, Taiwan. All irradiations were carried out at a beam current of 120 μA, which gave an average integrated current at the target of 300 μA h. After end of bombardment (EOB), the target was cooled for 6–8 h for the ^{123}Cs to decay to ^{123}Xe and transform further into ^{123}I. The target was washed with dilute NH_4OH (0.0016 N, 500 mL) and eluted with NH_4OH (0.16 N, 4 mL). The eluents were immediately loaded onto an alumina-B cartridge that had been pretreated with acetic acid (5.8 N, 10 mL). Followed by loading onto a second column of resin (AG50W-X8) that was pretreated with NaOH (1 N, 4 mL), the eluents were combined (2–3 mL) and a volume that ranged from 0.3 to 0.6 mL was used throughout the subsequent radiolabeling experiment. Radiolabeling was performed in a hood with sufficient ventilation and that had been fitted with a hepafilter for operation with ^{123}I. [^{123}I]IOFA **2** was purified by HPLC for which the components consisted of a Waters 510 pump, a linear UVIS detector (254 nm) that was placed in series with a Berthhold γ-flow detector on a ZORBAX SILcolumn (250 mm × 9.4 mm, 5 μm). The HPLC was run at 3 mL/min with MeOH/$CHCl_3$ 1:99 as the mobile phase. Quality analysis of [^{123}I]IOFA **2** was performed on the same HPLC setup. The settings for the radioactive ligand binding assay included a gel filtration column that consisted of TSKgel G3000PWxl 7.5 × 300 (mm) with a particle size of 10 μm, which was purchased from Tosoh Bioscience LLC. The corresponding eluting conditions including PBS buffer and flow rate of 1 mL/min were employed throughout the experiment. The identity of [^{123}I]IOFA **2** was confirmed using an authentic sample **2** on the HPLC chromatogram after coinjection. The peak area of the UV absorbance at 254 nm that should have corresponded to authentic sample **2** was calculated by interpolating a standard curve that related mass to UV absorbance. Only a specific activity of below 36 GBq/μmol could be measured accurately. Radioactive measurements were performed using a Capintec R15C dose calibrator.

All the in vivo experiments were performed in compliance with the NHMRC Taiwan Code of Practice for the care and use of animals for scientific purposes. Male Sprague–Dawley (SD) rats that were 49 weeks old were obtained from the Animal Research Center (Chang-Gung Memorial Hospital, Taiwan). The rats were housed under constant environmental conditions and were allowed free access to food and water throughout the experimental period. In vivo studies were performed in a thioacetamide-induced cholangiocarcinoma rat (37th week post administration) along with a normal rat as a control.

The rats were anaesthetized via inhalant isoflurane (Forthane, Abbott) in 200 mL/min oxygen during the imaging study. SPECT system (X-SPECT/CT, Gamma Media, Northridge, CA, USA) was used for small animal imaging experiments.

2.2. Chemical preparation

2.2.1. 4-(4′-iodobiphenyl-4-yl)-4-oxobutanoic acid **1**

A mixture of succinic anhydride (893 mg, 9.0 mmol) and $AlCl_3$ (2.52 g, 18.8 mmol, 2.1 eq) in CH_2Cl_2 (45 mL) was stirred at room temperature for 20 min while the mixture became a milky paste. The viscous mixture was moved to an ice bath and stirred in the dark for 2 min. Upon the addition of commercial 4-iodobiphenyl (2.5 g, 9.0 mmol), the mixture turned dark green. Stirring was then continued for 1 h. TLC (acetone:*n*-hexane = 3:7) was used to observe the consumption of iodobiphenyl ($R_f = 0.87$) and the formation of product **1** ($R_f = 0.21$). The mixture was poured into a mixture of HCl (12 N, 250 mL) in ice (500 g), and stirring was carried out until the dark green color disappeared, and yellow suspended solids were formed. After filtering the mixtures using a Büchner funnel, the residual solid was collected. The mixture was dissolved in aqueous NaOH (1 N, 250 mL). EtOAc was then added to partition the undesired organic impurities, which were then removed. The aqueous layer was collected and HCl (12 N) was added to acidify the solution until the solids precipitated. The mixture was transferred to a Büchner funnel where it was washed with distilled water to remove the rest of the acid. The residue was dried under reduced pressure, and a fruity yellow solid was obtained at a crude yield of 89% (3.0 g). Although additional purification using HPLC with various eluents was performed, identification of desired product **1** and the deiodinated byproduct was difficult. The ratio of iodo and deiodinated byproducts was determined through structural modification as described in the subsequent preparation. Calcd. $C_{16}H_{13}IO_3$ $[M]^+ = 379.99$, ESI + Q-TOF MS, $M = 380.0$ (m/z), $[M+Na]^+ = 403.0$, and $[2M+Na]^+ = 782.9$; ^{1}H NMR (500 MHz, CD_3OD): δ 2.89 (*t*, *J* = 6.5 Hz, 2H, aliphatic), 3.50–3.53 (*m*, 2H, aliphatic), 7.62–7.65 (*m*, 2H, Ar), 7.83–7.85 (*m*, 1H, Ar), 7.91–7.93 (*m*, 2H, Ar), 7.99 (*d*, *J* = 7.5 Hz, 1H, Ar), and 8.24 (*d*, *J* = 8.0 Hz, 2H, Ar).

2.2.2. 4-(4′-iodobiphenyl-4-yl)-N-octyl-4-oxobutanamide (IOFA) **2**

To a two-necked round-bottomed flask that contained a mixture of **1** in DMF (15 mL) was added HBTU (O-benzotriazol-1-yl-*N,N,N′,N′*-tetramethyluronium hexafluorophosphate; 998 mg, 2.6 mmol) and diisopropyl ethylamine (680 mg, 0.9 mL, 5.2 mmol, 2 eq) in sequence. Stirring was then carried out for 30 min after which commercial octan-1-amine (510 mg, 3.9 mmol, 1.5 eq) was added. Stirring was then carried out for another 15 min. TLC (acetone/*n*-hexane = 3:7) was used to observe the consumption of the starting material **1** ($R_f = 0.21$) and the formation of the product **2** ($R_f = 0.56$). The mixture was concentrated under high vacuum at 60 °C. The residue was partitioned between aqueous HCl (1 N, 30 mL × 2) and $CHCl_3$ (50 mL). The organic layers were combined and then concentrated under reduced pressure. The residue that was obtained was purified by using flash chromatography with an eluent of acetone/$CHCl_3$ = 1:29 to provide pale yellow solid **2** with a plastic-like smell at 73% yield (938 mg). An analytic sample was fractionated by HPLC with an eluent of MeOH/$CHCl_3$ = 1:99, t_R = 17.3 min white solid, mp: 181–182oC; Calcd. $C_{24}H_{30}INO_2$ $[M]^+ = 491.1$, ESI + Q-TOF MS, $M = 491.1(m/z)$, $[M+H]^+ = 492.1$, and $[M+Na]^+ = 514.1$; HRMS-ESI, Calcd. $[M+H]^+$ = 492.13995 and $[M+Na]^+$ = 514.12189; found: $[M+H]^+ = 492.13955$ and $[M+Na]^+ = 514.12173$; ^{1}H NMR (500 MHz, $CDCl_3$): δ 0.87 (*t*, *J* = 7.0 Hz, 3H, octyl, CH_3), 1.26–1.32 (*m*, 10H, octyl, CH_2), 1.50 (*t*, *J* = 7.0 Hz, 2H, Octyl, CH_2), 2.62 (*t*, *J* = 6.5 Hz, 2H, aliphatic, CH_2), 3.24 (*q*, *J* = 7.0 Hz, 2H, octyl, CH_2), 3.39 (*t*, *J* = 7.0 Hz, 2H, aliphatic, CH_2), 5.77 (bs, 1H, amide), 7.35 (*d*, *J* = 8.5 Hz, 2H, Ar), 7.63 (*d*, *J* = 8.0 Hz, 2H, Ar), 7.79 (*d*, *J* = 8.5 Hz, 2H, Ar), and 8.05 (*d*, *J* = 8.5 Hz, 2H, Ar); ^{13}C NMR (125 MHz, $CDCl_3$): δ 14.07 (Octyl-CH_3), 22.62 (Octyl, CH_2), 26.88 (Octyl, CH_2), 29.18 (Octyl, CH_2), 29.23 (Octyl, CH_2), 29.59 (Octyl, CH_2), 30.37 (Octyl, CH_2), 31.76 (NH–CO–CH_2), 34.21 (Ar–CO–CH_2), 39.68 (CO–NH–CH_2), 94.28 (Ar, C–I), 127.00 (Ar, CH), 128.78 (Ar, CH), 129.00 (Ar, CH), 135.61 (Ar, C–CO), 138.06 (Ar, CH), 139.32 (Ar, C–Ar), 144.69 (C–Ar), 171.88 (NH–CO), and 198.64 (Ar–CO).

2.2.3. N-octyl-4-oxo-4-(4′-(trimethylstannyl)biphenyl-4-yl)butanamide **3**

To a flask (10 mL) containing IOFA **2** (100 mg, 0.2 mmol) in 1,4-dioxane (1 mL) bis(triphenylphosphine)palladium dichloride (5 mg, 0.007 mmol, 0.03 eq) and hexamethylditin (237 mg, 0.15 mL, 0.72 mmol, 3.6 eq) were added sequentially. The mixture was warmed to 85 °C, and stirring was carried out for 15 min. TLC (acetone/$CHCl_3$ = 1:19) was used to follow the consumption of the starting material **2** ($R_f = 0.50$) and the formation of the product **3** ($R_f = 0.55$). The mixture was filtered through a celite pad, and the filtrates were concentrated under reduced pressure. The residue that was obtained was purified using flash chromatography with the eluent EtOAc/*n*-hexane = 2:8 to provide a white paste **3** at 56% yield (61 mg). An analytic sample was obtained through fractionation with HPLC using an eluent of EtOAc/*n*-hexane = 1:1, t_R = 11.0 min. The product smelled like the combination of plastic and acid. Calcd. $C_{27}H_{39}NO_2Sn$ $[M]^+ = 525.20$ (41.5%), 527.20 (75.4%), 528.20 (44.8%), 529.20 (100.0%), ESI + Q-TOF MS, $[M+H]^+ = 526.0$ (29%), 528.1 (71%), 529.0 (43%), and 530.1 (100%); HRMS-ESI, Calcd. $[M+H]^+$ = 530.20810 and $[M+Na]^+ = 552.19005$; found: $[M+H]^+ = 530.20767$ and $[M+Na]^+ = 552.19021$; ^{1}H NMR (500 MHz, C_6D_6): δ 0.25 (*t*, *J* = 27.5 Hz, 9H, Sn–CH_3), 0.89 (*t*, *J* = 7.5 Hz, 3H, aliphatic), 1.14–1.20 (*m*, 8H, aliphatic), 1.25–1.30 (*m*, 4H, aliphatic), 2.39 (*t*, *J* = 6.5 Hz, 2H, aliphatic), 3.12–3.17 (*m*, 4H, aliphatic), 5.11 (bs, 1H, amide), 7.15–7.50 (*m*, 6H, Ar), and 7.95 (*d*, *J* = 8.5 Hz, 2H, Ar); ^{13}C NMR (125 MHz, $CDCl_3$): δ −9.55 (Sn–CH_3), 14.06 (Octyl-CH_3), 22.61 (Octyl, CH_2), 26.88 (Octyl, CH_2), 29.17 (Octyl, CH_2), 29.23 (Octyl, CH_2), 29.57 (Octyl, CH_2), 30.41 (Octyl, CH_2), 31.75 (NHCO–CH_2), 34.22 (NHCO–CH_2), 39.66 (CONH–CH_2), 126.70 (Ar, CH), 127.17 (Ar, CH), 128.66 (Ar, CH), 135.23 (Ar, C–CO), 136.40 (Ar, CH), 139.62 (Ar, C–Sn), 142.69 (Ar, C–Ar), 145.95 (Ar, C–Ar), 171.97 (CO–NH), 198.70 (Ar–CO).

2.3. Preradiolabeling of organostannyl compound **3** with non-radioactive NaI

A sample vial (50 mL) that contained NaI (7.8 mg, 0.052 mmol, 7.5 eq) and doubly distilled water (0.5 mL) was sonicated for 2 min. A solution of glacial AcOH and 30% H_2O_2 (1:1.5 v/v) was added, and sonication was carried out for a further 1 min. After adding the solution of organostannyl compound **3** (4 mg, 0.007 mmol, 1 eq) in CH_2Cl_2 (2 mL) the mixture was sonicated for 20 min. The quenching reagent $Na_2S_2O_3$ (0.1 M, 10 mL) was then added. Next, the mixture was partitioned by using H_2O (5 mL) and CH_2Cl_2 (10 mL). The organic layer was collected for subsequent loading onto a neutral alumina cartridge followed by washing with a solution of CH_2Cl_2 and MeOH (2:1, v/v, 10 mL). After being concentrated under reduced pressure, the residue was purified with HPLC (Si-100) using the eluent CH_2Cl_2:MeOH = 99:1 to provide the desired fractionations: t_R = 17.2 min for compound **2** and t_R = 18.2 min for the destannylated byproduct OFA (see also the radiochemical labeling section). After being concentrated under reduced pressure, the desired compound **2** was obtained at 50% yield (2 mg).

2.4. Radiochemical labeling of 4-(4′-[^{123}I]iodobiphenyl-4-yl)-N-octyl-4-oxobutanamide [^{123}I]IOFA 2

To a round-bottomed flask (25 mL) that was charged with a mixture of aqueous [^{123}I]NaI (75 mCi) in H_2O (less than 0.6 mL), glacial AcOH (3.5 mL) and H_2SO_4 (0.06 mL) were added sequentially. Stirring was then carried out for 1 min. A mixed solution (3.5 mL) of glacial AcOH and aqueous H_2O_2 (30% wt) at a ratio of 2:3 (v/v) was added and the mixture was vigorously stirred for 1 min. A solution of organostannyl compound **3** (9 mg) in CH_2Cl_2 (1 mL) was then added, and the mixture was vigorously stirred at room temperature for 20 min. The reaction was quenched by adding $Na_2S_2O_3$ (2 M, 0.8 mL). The mixture was then partitioned and the organic layer was collected, and the residual aqueous layer was back-extracted with CH_2Cl_2 (1 mL) twice. The organic layers collected were treated with seven large spatulas worth of Na_2SO_4 and then gravity filtered. The filtrates were loaded onto a CH_2Cl_2-preconditioned Alumina N cartridge followed by washing with a mixed solution of

Please cite this article in press as: Huang H-L, et al., [^{123}I]Iodooctyl fenbufen amide as a SPECT tracer for imaging tumors that over-express COX enzymes, Biomaterials (2013), http://dx.doi.org/10.1016/j.biomaterials.2013.01.050

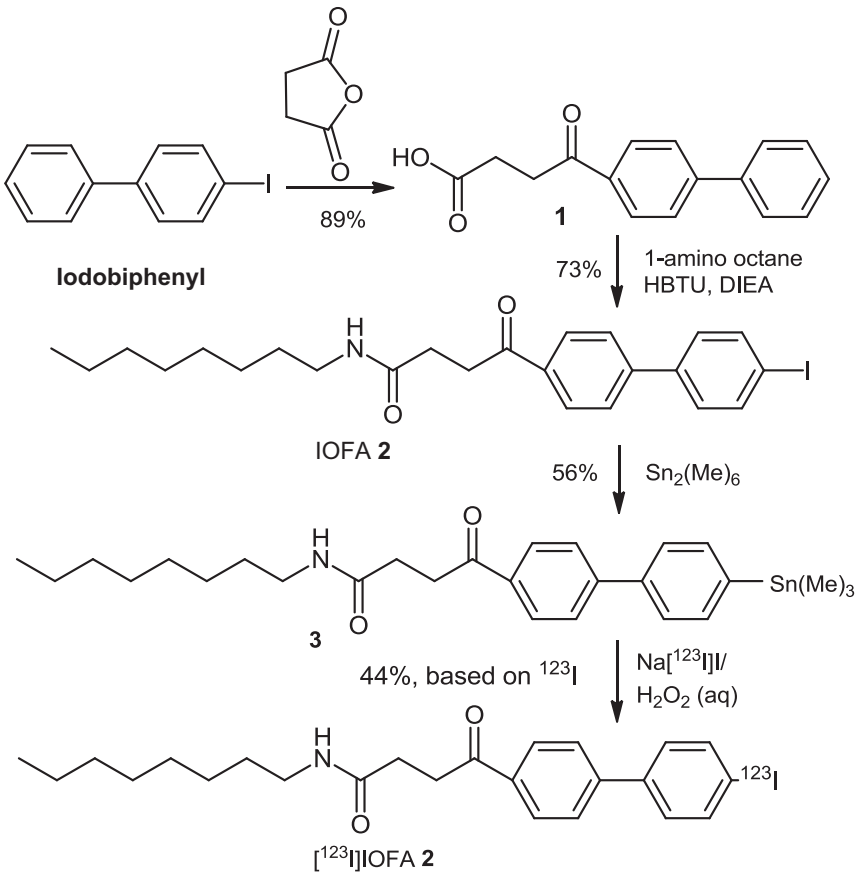

Scheme 1. Preparation of radioiodolabeled [^{123}I]IOFA **2**.

CH_2Cl_2 and MeOH (3 mL, 2:1 v/v). The filtrates were concentrated under reduced pressure, and the residue was further purified with HPLC using the eluent MeOH/$CHCl_3$ = 1:99, t_R = 15.0 min (Radio). Fractions of [^{123}I]iodooctafenbufen **2** that had been isolated from several injections were combined followed by concentration under reduced pressure to provide [^{123}I]**2** at 15% radiochemical yield (8.1 mCi, decay corrected). The specific radioactivity and radiochemical purity were 36 GBq/μmole and 99%, respectively. Regarding animal SPECT imaging, the cholangiocarcinoma tumor-bearing rat and control rat were each injected with 0.76 mCi/1 mL and 1.39 mCi/1 mL, respectively.

2.5. Bioassay of competitive inhibition of the substrate transfer (CIST) by COX

The procedure, as stated by the product supplier, was adopted throughout the whole assay. In brief, inhibitors were diluted with ethanol to final working concentrations that ranged either from 10^{-3}–10^{3} μM for positive controls SC560 and SC58125 or from 10^{-1}–10^{5} μM for IOFA **2**, fenbufen, and uridine, respectively. The assay buffer (4 mL) was diluted with double distilled H_2O (36 mL) to provide the stock solution of assay buffer. The heme solution (88 μL) was diluted with the above stock solution of assay buffer (1.91 mL). Each of the stock solutions (200 μL)

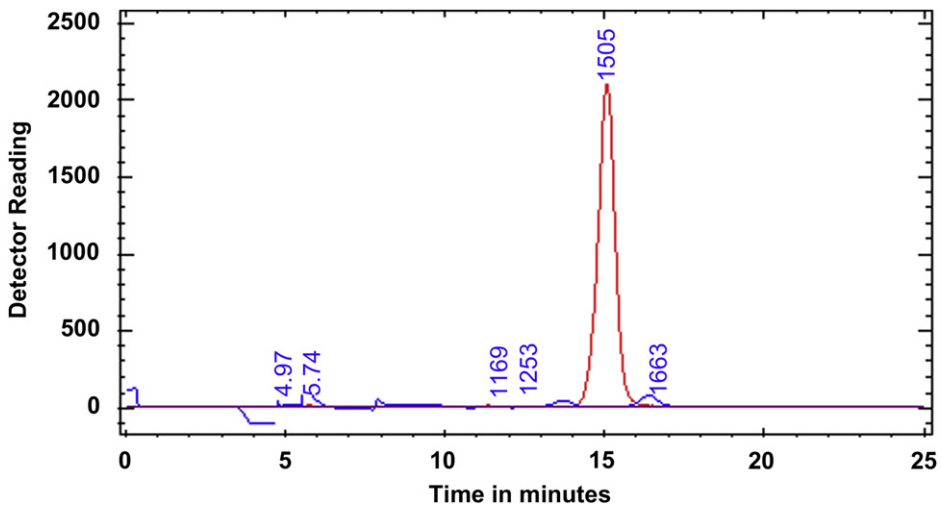

Fig. 2. HPLC chromatogram for [^{123}I]IOFA **2** (15.05 min) prior to HPLC purification. A normal phase column (Si-100) was employed. Red line: radioactivity and blue line: UV signal at 254 nm. (For interpretation of the references to color in this figure legend, the reader is referred to the web version of this article.)

Please cite this article in press as: Huang H-L, et al., [^{123}I]Iodooctyl fenbufen amide as a SPECT tracer for imaging tumors that over-express COX enzymes, Biomaterials (2013), http://dx.doi.org/10.1016/j.biomaterials.2013.01.050

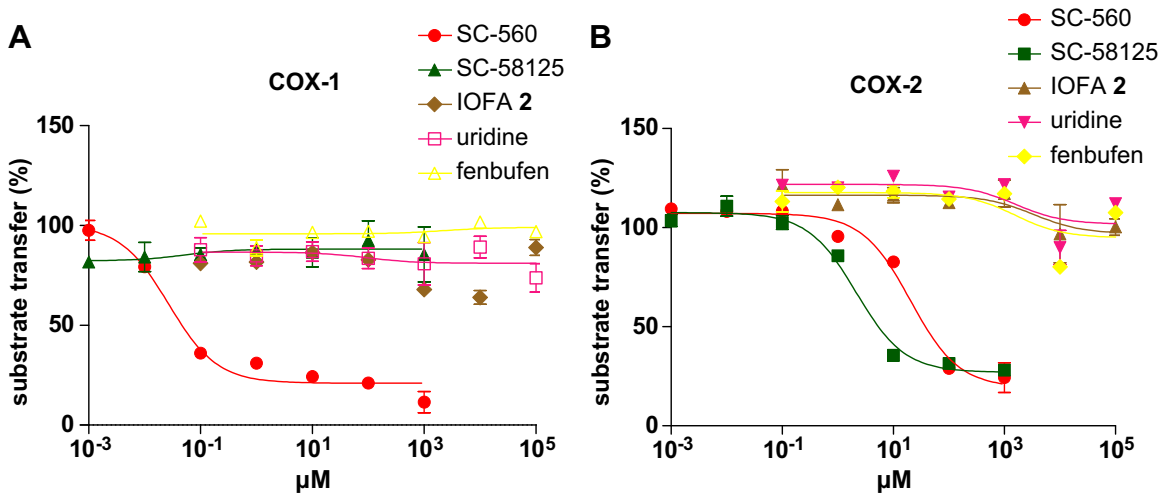

Fig. 3. Inhibition of substrate transfer by COX-1 (A) and COX-2 (B) in the presence of compounds that were tested at various concentrations. Uridine was used as a negative control, whereas Sc-560 and Sc-58125 were used as COXs and COX-2 inhibitors, respectively. Triplicated measurements were performed for each concentration of compounds.

of COX-1 or COX-2 was added to the above assay buffer (400 μL). All of the reagents including the stock solutions of enzyme, heme, arachidonic acid, and the colorimetric substrate *N,N,N′,N′*-tetramethyl-1,4-benzenediamine dihydrochloride product (TMPD) were cooled in a box that contained dry ice. In addition to uridine and IOFA **2** that were dissolved in H_2O and DMSO, respectively, the other compounds were dissolved in EtOH. After mixing the above stock solutions of COX (10 μL), heme (10 μL), compound tested (10 μL), assay buffer (150 μL), AA (20 μL) and TMPD (20 μL) to make a total volume of 220 μL. The serial dilution was performed in a 96-well microtiter plate. The absorbance of each of the well was measured using UV detector at $\lambda_{max} = 595$ nm. The software GraphPad 5 was used to plot the absorption vs. concentration. The percentage inhibition was calculated as $\{1 - [(Abs_{initial} - Abs_{BKG(assay\ buffer+EtOH)}) - (Abs_{initial+C.T.} - Abs_{BKG(assay\ buffer+C.T.)})]/[(Abs_{AA+COx} - Abs_{BKG(assay\ buffer+EtOH)})]\} \times 100\%$. BKG: background, C.T.: compounds tested.

2.6. Radioligand binding assay

An aliquot (10 μL) was drawn from the commercial stock solution of COXs (200 μL). An additional 80 μL of Tris buffer (0.1 M, pH = 8.0) was added to it. The diluted solutions (90 uL) of COX-1 or COX-2 each were added by the radiotracer [^{123}I] IOFA **2** in EtOH, whereby the concentration ranged from 66 μCi/10 μL to 70 μCi/10 μL. The whole mixture (100 μL) was incubated at 25 °C for 15 min followed by purification using HPLC coupled with gel filtration column. PBS buffer (0.1 M, pH = 7.3) was employed as the eluent, and the flow rate was 1 mL/min.

2.7. Small animal CT/SPECT imaging study

All in vivo experiments were performed in compliance with the NHMRC Taiwan Code of Practice for the care and use of animals for scientific purposes. Male Sprague–Dawley (SD) rats that were 49 weeks old were obtained from the Animal Research Center (Chang-Gung Memorial Hospital, Taiwan). The rats were housed under constant environmental conditions and were allowed free access to food and water throughout the experimental period. In vivo studies were performed in a thioacetamide (TAA)-induced cholangiocarcinoma rat (37th week post administration) along with a normal rat as a control.

The rats were anaesthetized via inhalant isoflurane (Forthane, Abbott) in 200 mL/min oxygen during the imaging study. The imaging study was carried out at the Nuclear Energy Research Institute. SPECT system (X-SPECT/CT, Gamma Media, Northridge, CA, USA) was used for the small animal imaging study. The crude data that was taken from the imaging study were further treated with Preclinical Multi-Modality Data Analysis software (ver 3.2; PMOD Technologies Ltd, Zurich, Switzerland).

Table 1
Comparison of IC_{50} values that were obtained from the present assay and the literature.

Substrate	IC_{50} value			
	COX-1 (μM)		COX-2 (μM)	
	This assay	Lit. data	This assay	Lit. data
IOFA **2**	>10	N.A.	>10	N.A.
Resveratrol	3.9	1.56[a]	50	0.99[b]
SC-58125	>10	>10[c]	5	0.05[c]
SC-560	0.060	0.009[d]	2.5	6.3[d]
Uridine	>10	N.A.	>10	N.A.
Fenbufen	>10	3.9[e]	>10	8.1[e]

[a] Ref. [47].
[b] Ref. [48].
[c] Ref. [49].
[d] Ref. [50].
[e] Ref. [45].

2.8. MTT assay (cell viability assay)

The cell toxicity was assessed by a viability assay, MTT (3-(4,5-dimethyl-thiazol-2-yl)-2,5-diphenyl tetrazolium bromide) reduction. In brief, T98 (human glioma cell line) cells were plated in the 96-well plate (5000/well) and maintained at 37 °C, 5% CO_2 incubator with MEM, 10% fetal calf serum (Gibco, USA). After 24-hour pulse with IOFA, 50 μL of MTT (5 mg/mL) was added to each well for four hours. After removal of medium, 100 μL of DMSO was added to each well and the optical absorbance was determined by a spectrophotometry using a plate reader at 570 nm.

3. Results and discussion

3.1. Radiochemical synthesis

Fenbufen analogs have seldom been reported except for their use in an anti-inflammatory assay of a fenbufen amide library [45]. This might be probably due to its relatively limited structural variability. The reactor-generated radioactive iodide ([^{123}I]I^-) could be introduced into OFA using a carbon on the aromatic ring. The precursor organostannyl compound **3** was thus prepared via the dehalostannylation of iodooctyl fenbufen amide (IOFA) **2** as outlined in Scheme 1.

Nonradioactive IOFA **2** was used to prepare organostannyl compound **3** followed by radioiododestannylation to provide radioactive [^{123}I]IOFA **2** (Scheme 1). The very low polarity of IOFA **2** limited the choice of the eluent during column chromatography. Thus, HPLC was virtually the only tool that was available for purifying IOFA **2** in spite of its limited capacity of 10 mg for each injection. Radiochemical synthesis of [^{123}I]IOFA **2** was relatively straightforward. During the workup, a sufficient amount of drying agent of Na_2SO_4 was needed. Furthermore, incomplete removal of the residual acetic acid after it was concentrated under reduced pressure was a formidable problem. Thus, an additional procedure for extracting, drying, and concentrating was repeated until the final white solid became odorless.

Please cite this article in press as: Huang H-L, et al., [^{123}I]Iodooctyl fenbufen amide as a SPECT tracer for imaging tumors that over-express COX enzymes, Biomaterials (2013), http://dx.doi.org/10.1016/j.biomaterials.2013.01.050

The poor solubility of IOFA **2** in the water-phase based saline solution constituted another challenge because [^{123}I]IOFA **2** was obtained as a white solid after HPLC purification. Prior to injecting it into the tail vein for subsequent animal imaging, the saline solution turned cloudy. Hence, the suspended white particles were filtered twice by using 0.45-μM filters. The relatively low specific activity of [^{123}I]IOFA **2** of less than 37 GBq/μmol was due to the presence of a trace amount of an unknown UV-inactive white solid, which may have decreased its specific activity (Fig. 2).

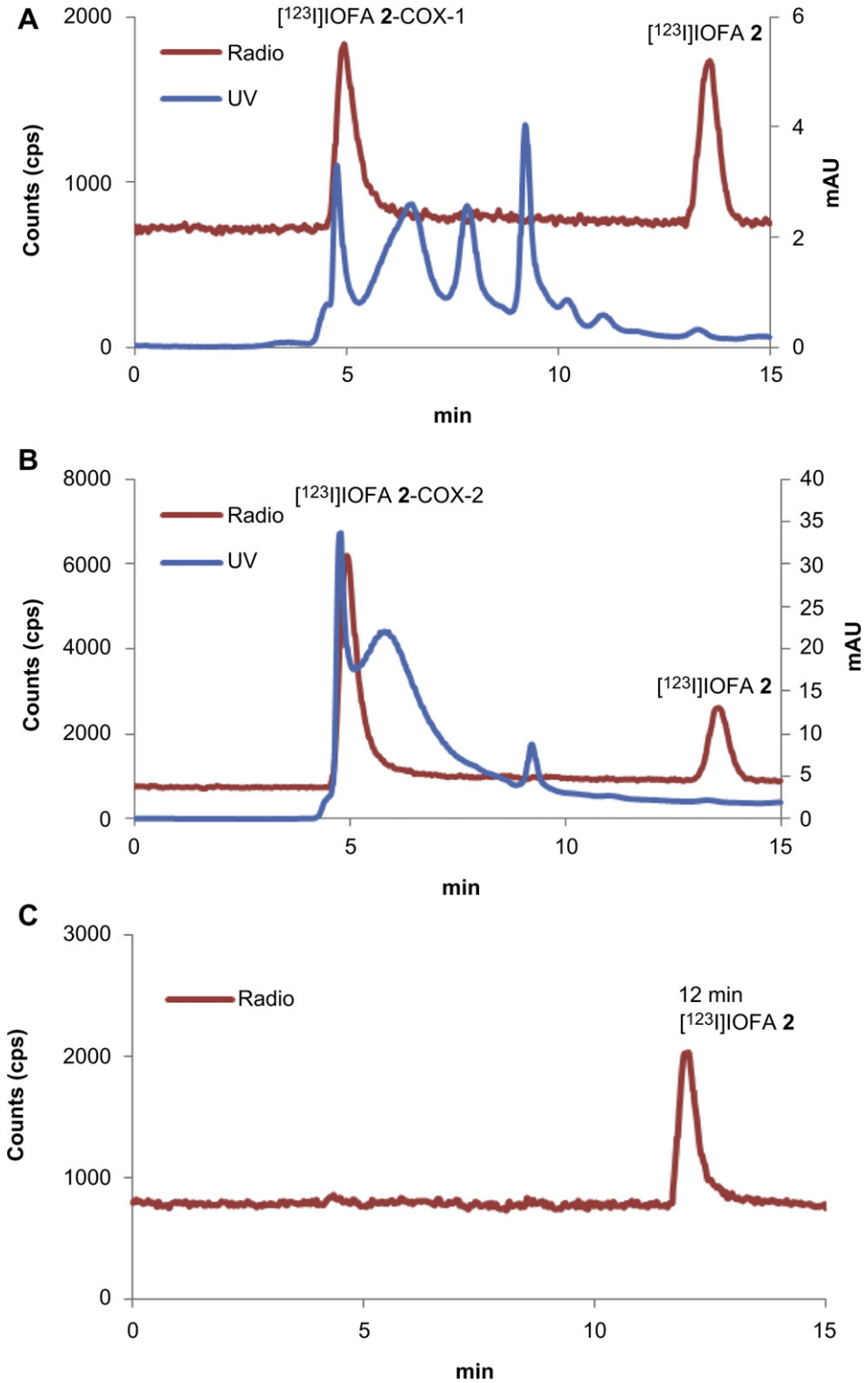

Fig. 4. HPLC chromatograms of a mixture of [^{123}I]IOFA **2** with (A) COX-1 enzyme and (B) COX-2 enzyme. Binding yield = peak area at 5 min/(peak area at 5min + peak area at 13.6 min). CPS: counts per second. (A) [^{123}I]IOFA-COX-1 bound conjugate (t_R = 5.0 min) and residual unbound [^{123}I]IOFA **2** (t_R = 13.6 min) where the binding yield was 56% and 44% of the intact form [^{123}I]IOFA **2** remained (13.6 min). (B) [^{123}I]IOFA-COX-2 bound conjugate (t_R = 5.0 min) and residual unbound [^{123}I]IOFA **2** (t_R = 13.6 min) where the binding yield was 79% and 21% of the intact form remained (13.6 min). (C) Chromatogram of solo injection of [^{123}I]IOFA **2**. Retention time = 12.0 min.

Please cite this article in press as: Huang H-L, et al., [^{123}I]Iodooctyl fenbufen amide as a SPECT tracer for imaging tumors that over-express COX enzymes, Biomaterials (2013), http://dx.doi.org/10.1016/j.biomaterials.2013.01.050

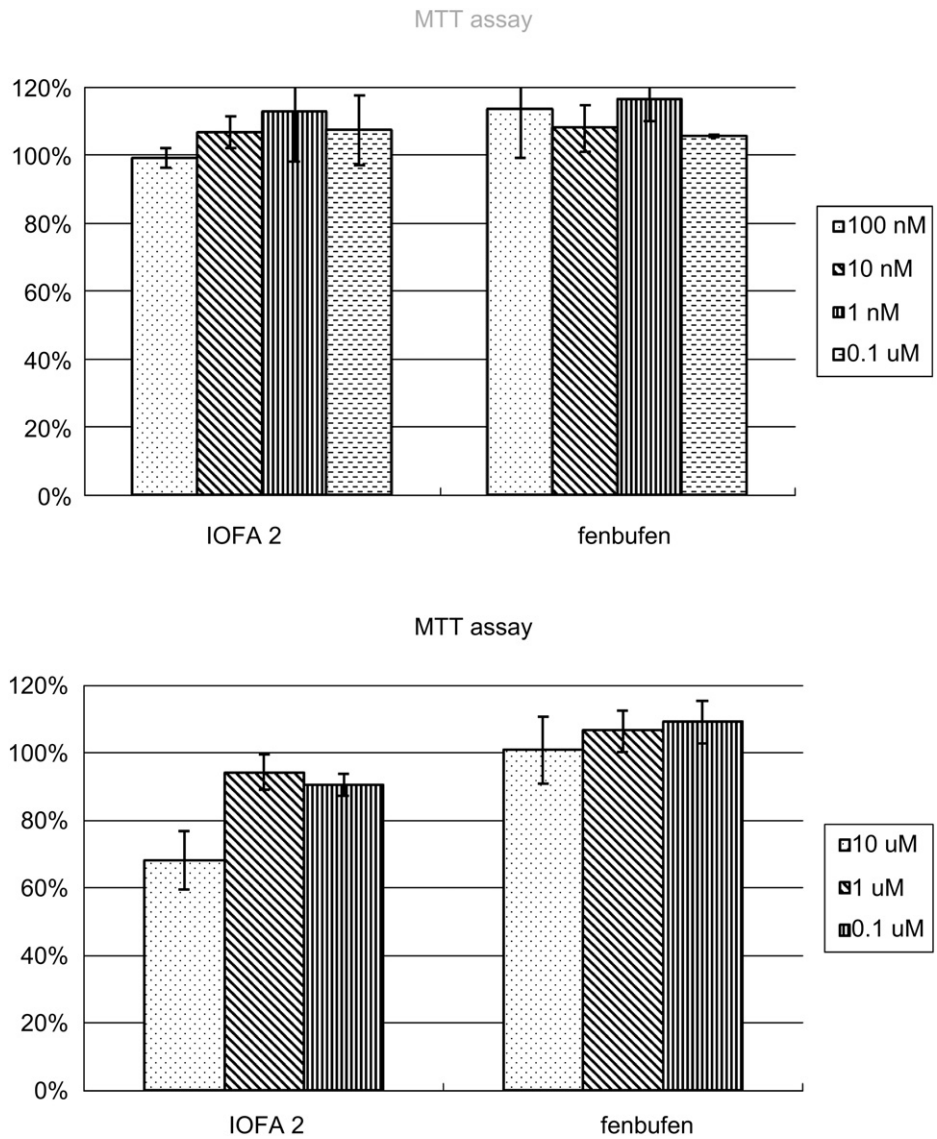

Fig. 5. Cell survival assay (MTT assay) of IOFA **2**.

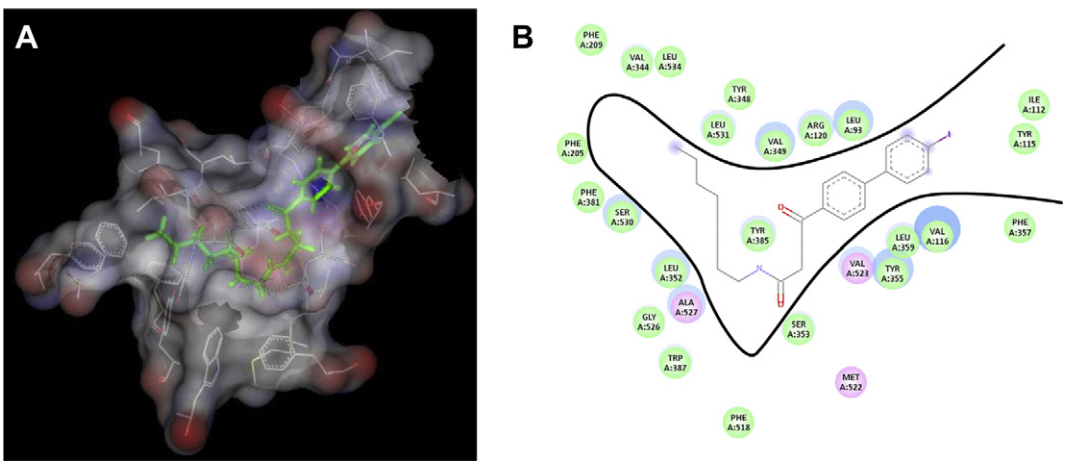

Fig. 6. Molecular docking of IOFA **2** and COX-2. The side chain was extended into the channel behind the lobby occupied by the diaryl ring. (A) Illustration by electrostatic map. (B) The 2-D illustration indicated the surrounded amino acid residues. Software: Discovery Studio 2.1 with Ligandfit. Active site was defined by using flurbiprofen complex of PDB entry of 3RR3.

Please cite this article in press as: Huang H-L, et al., [^{123}I]Iodooctyl fenbufen amide as a SPECT tracer for imaging tumors that over-express COX enzymes, Biomaterials (2013), http://dx.doi.org/10.1016/j.biomaterials.2013.01.050

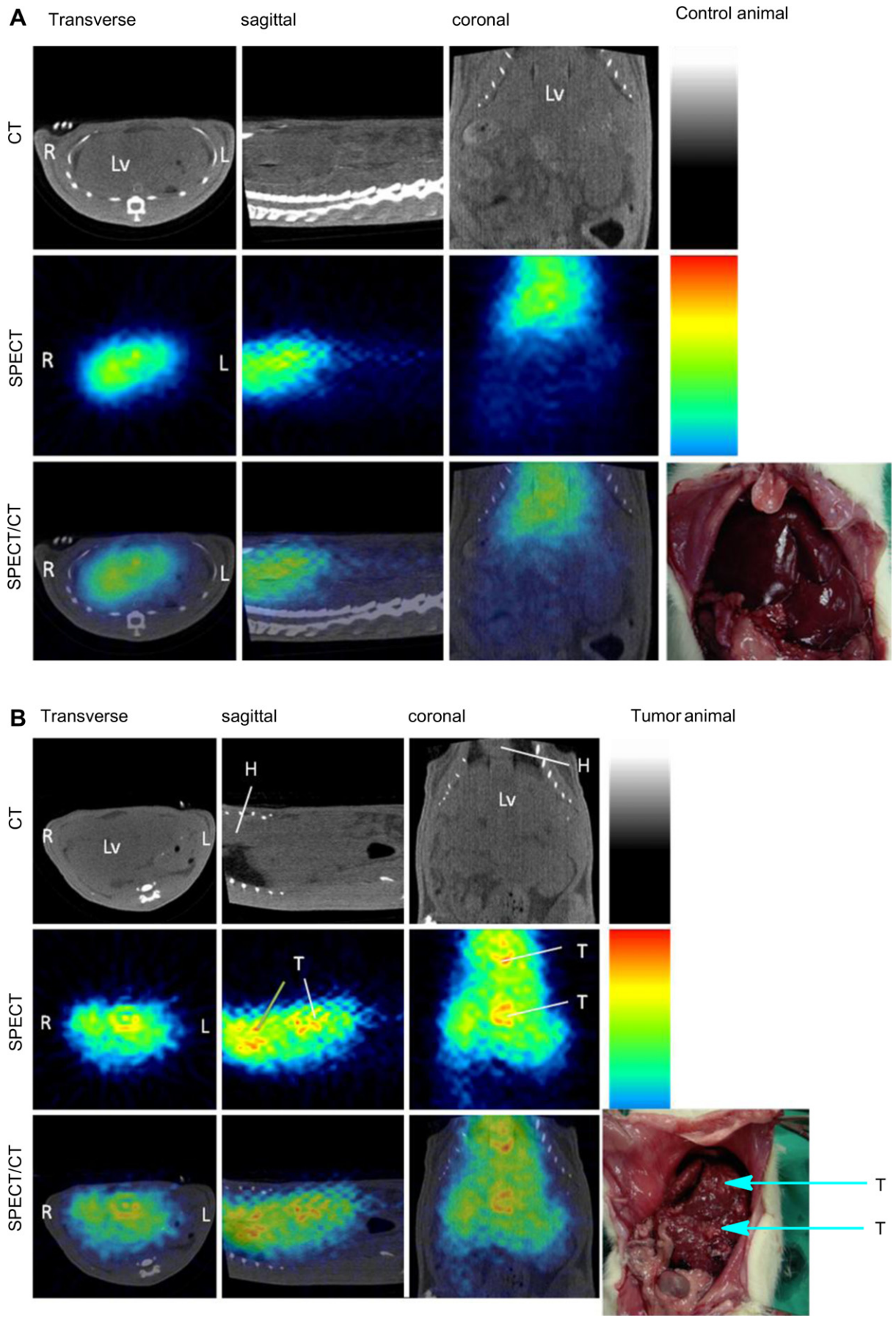

Fig. 7. (A). SPECT/CT images of the normal rat with [^{123}I]IOFA **2** were summated from 30 to 60 min post injection. The injection dose was 1.39 mCi/1 mL. Lv: Liver, (B) SPECT/CT images of the CCA rat (feeding with TAA for 37 weeks) were summed from 30 min to 60 min post injection. The injection dose was 0.76 mCi/1 mL. Lv: liver, H: heart, T: tumor.

Please cite this article in press as: Huang H-L, et al., [^{123}I]Iodooctyl fenbufen amide as a SPECT tracer for imaging tumors that over-express COX enzymes, Biomaterials (2013), http://dx.doi.org/10.1016/j.biomaterials.2013.01.050

3.2. Bioassay of competitive inhibition of the substrate transfer (CIST) by COX enzymes

Both the COX-2 selective (SC-58125) and highly COX active but not selective (SC-560) inhibitors were used as controls throughout the assay (Fig. 3). The assay results showed that IOFA **2** displayed marginal competitive inhibition against the reduction of the colorimetric substrate by COX-1 and COX-2.

The present assay was based on assessing the reduction potential that was catalyzed by POX, which was responsible for the second catalysis of COX. Furthermore, two intermediates were generated from the AA-heme-COX complex that could oxidize *N,N,N′,N′*-tetramethyl-1,4-benzenediamine dihydrochloride (TMPD) to provide the colorimetric product [11,46]. It has been speculated that POX inactivation involves the oxyferryl heme group, whereas COX inactivation involves a tyrosyl radical [46]. Both of the two positive controls could potentially inhibit POX and thereby block COX function (Table 1). Specifically, COX-2 inhibition is caused by binding to E_{cat}. These inhibitors are thus classified as being competitive inhibitors. Clearly, IOFA **2** was not one such competitive inhibitor.

As a result, the binding affinity of the substrate toward the first catalytic binding site could not be evaluated very well. Another method that entailed using radioligand binding assay was therefore adopted as is described below.

3.3. Radioligand binding assay

The basis of the assay was based on the differential retention times for HPLC of the radioligand-enzyme complexes and the unbound radioligand. Prior to submitting the binding product mixtures for HPLC analysis, a small aliquot of enzyme (10 μL) from the commercial stock solution (200 μL) was introduced to ensure the formation of enough radioligand–enzyme complex prior to analysis. The pronounced nonpolarity of the radioligand [^{123}I]IOFA **2** might prevent using polar eluents for chromatography. For us, a water-based PBS buffer as an eluting solvent did not alter the retention time of [^{123}I]IOFA **2**. The chromatogram showed an expected pattern in that unbound [^{123}I]IOFA **2** with a smaller molecular size was retarded due to its elution through the miniaturized fractured path (Fig. 4). In contrast, the bound complex with its larger molecular size should have been eluted along the main fractured path thereby traveling at a more rapid speed.

Whereas the substrate transfer (CIST) assay showed that IOFA **2** was neither a potent nor selective COX inhibitor, the radioligand binding assay as shown above (Fig. 4), indicated its preferential binding affinity toward COX-2 rather than COX-1. Its affinity ratio was 1.4:1 when calculated from radioactivity fraction of 76% vs. 56%. Because IOFA **2** did not exhibit a competent inhibition profile similar to that of traditional COX-2 inhibitors, the binding site should be confined to E_{allo}. Its role in regulation might be similar to common non-substrate FAs. Interestingly, IOFA **2** exhibited a cell-growth inhibition profile when acting against T98 cells (30% inhibition at 10 μM, Fig. 5) that differentiates it from common non-substrate FAs. Modeling was used to correlate its structure and reactivity (Fig. 6A). Of note, we observed close contact between Tyr^{385} and the amido hydrogen, which might compete with AA to carry out hydrogen abstraction during the first rate-determining step of COX activity (Fig. 6B). In addition, the biphenyl ring of IOFA **2** mimics the cyclopentane ring of oxidized AA that is formed from the addition of oxygen to AA, which constitutes the second rate-determining step. Thus, IOFA **2** seems to displace AA in terms of COX binding but does not appear to inhibit the formation of the radical cation of Tyr^{385}-heme complex as in the case of POX inhibitors. As shown in Fig. 6B, the 8-carbon side chain of IOFA **2** was capable of extending into a narrow bag in the active site that could induce a foot-like fit with the structure of IOFA **2**. The foot-like conformation of the IOFA-COX complex may mimic the L-shape conformation of the AA-COX complex. The stabilization that was

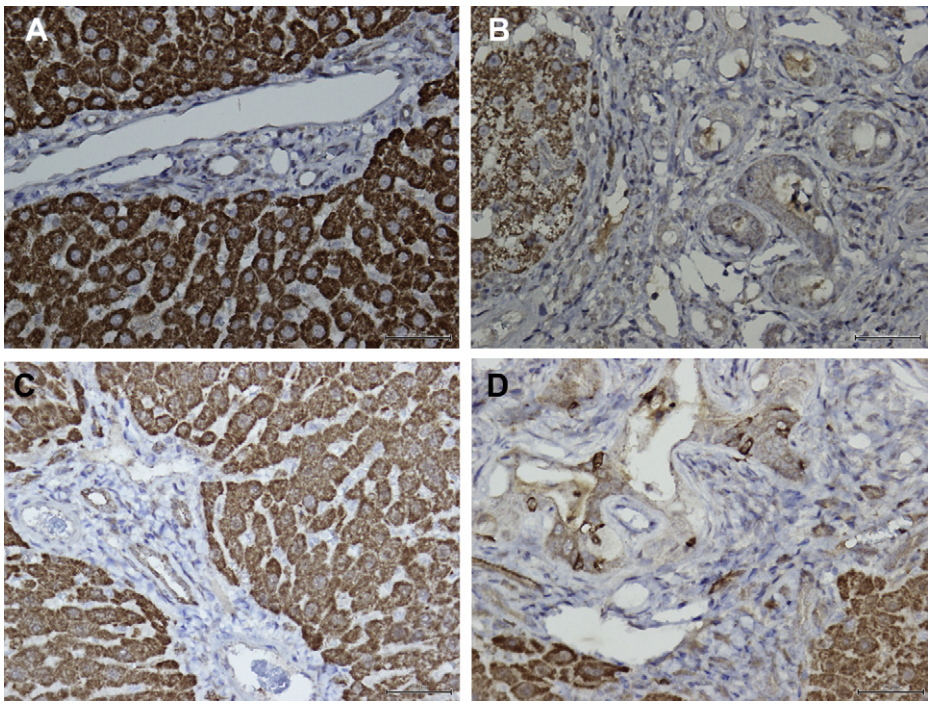

Fig. 8. Immunostaining study: (A) Negative cytoplasmic immunostaining of COX-1 of a normal bile duct of a normal rat (×400). (B) Positive cytoplasmic immunostaining of COX-1 of a CCA rat (×400). (C) Negative cytoplasmic immunostaining of COX-2 of a normal bile duct of a normal rat (×400). (D) Positive cytoplasmic immunostaining of COX-2 of a CCA rat (×400).

Please cite this article in press as: Huang H-L, et al., [^{123}I]Iodooctyl fenbufen amide as a SPECT tracer for imaging tumors that over-express COX enzymes, Biomaterials (2013), http://dx.doi.org/10.1016/j.biomaterials.2013.01.050

gained by fitting the octyl side chain might have triggered apoptotic signaling as described for AEA. To serve as a noninvasive imaging tracer in vivo, the binding complex should be durable during imaging processing. In an in vitro monitoring by HPLC with gel filtration column, about half of the radioactivity of the binding complexes was still intact after incubation for 40 min (data not shown). With this information in mind, the subsequent in vivo imaging frame was therefore set from 30 min to 60 min post *iv* injection.

3.4. Tumor imaging

Cholangiocarcinoma (CCA) tumor rat [51–57] was injected with an aliquot of [^{123}I]IOFA **2** (0.76 mCi/1 mL) via tail vein to obtain 1 h worth of SPECT imaging data (Fig. 7 (A)). The normal rat was injected with the residual aliquot of [^{123}I]IOFA **2** in a dose of 1.39 mCi/1 mL (Fig. 7 (B)). Although the two injections were conditioned by adjusting the solvent volume to attain equivalent specific activities, the normal rat received more specific activity. The in vivo distribution of radioactivity in the normal rat showed a homogeneous pattern, that was localized mainly in the liver and partly in the heart 30 min post administration (Fig. 7A). In contrast, a heterogeneous distribution was observed in the liver of the CCA tumor rat. Moreover, those regions that showed hot spots as indicated were equivalent to the white matter in the photograph that was taken of the same rat after it was sacrificed ((Fig. 7B), right lower corner). The white matter is an indication of the tumor lesion as judged on the basis of the clinical experience.

Specimens of the liver from each of the two rats were further analyzed by histological stainings against both COX-1 and COX-2 (Fig. 8). Clearly, the positive stainings of both the COX-1 and COX-2 were solely found in the bile duct of CCA tumor rat but not of the normal rat. The higher radioactivity accumulation in CCA rat may be because of a higher expression level of COX (s) or because of mutant COX (s) with higher binding activity. The latter assumption needs to be confirmed in a future study and could not be overridden by the current study. Although [^{123}I]IOFA **2** exerted a mixed COX binding affinity pattern (Fig. 4), the accumulation of a considerable amount of radioactivity in the heart was remarkable (Fig. 7B).

4. Conclusion

A 4-step facial synthesis was employed to provide [^{123}I]IOFA **2**. A radiochemical yield of 15% and a specific activity of less than 37 GBq/μmol were acceptable for SPECT imaging. The binding analysis of [^{123}I]IOFA **2** and COX using HPLC in conjugation with a gel filtration column showed preferable affinity toward COX-2 compared to COX-1. The results from both the noninvasive SPECT images of [^{123}I]IOFA **2** in the CCA tumor rat and the photographs after it was sacrificed were correlated with each other with respect to the hot spots and white matters in the tumor lesion. The expression levels of both COXs in the livers of the CCA tumor rat were significantly higher than that of the normal rat in terms of immunohistological staining. The marked accumulation of radioactive [^{123}I]IOFA **2** clearly demonstrated its potential as an imaging agent for diagnosing tumors. Tumor-associated inflammation could be imaged using [^{123}I]IOFA **2** by SPECT as well.

Acknowledgments

We are grateful to the National Science Council of Taiwan, CGMH_NTHU Joint Research, and Chang-Gung Medical Research Project for providing financial support through grant numbers NSC-100-2113-M-007-003, NSC-97-2314-B-182A-020-MY3, NSC-97-2314-B-182A-020-MY3, CGTH96N2342E1, CMRPG3B0581, CMRPG390661, CMRPG390931, and CMRPG3B0361. We also acknowledge the technical assistance that was provided by Mr. Yean-Hung Tu and Mr. Chun-Ming Shi.

Appendix A. Supplementary data

Supplementary data related to this article can be found at http://dx.doi.org/10.1016/j.biomaterials.2013.01.050.

References

[1] Wang X, Baek SJ, Eling T. COX inhibitors directly alter gene expression: role in cancer prevention? Cancer Metastasis Rev 2011;30:641–57.
[2] Kitamura T, Kawamori T, Uchiya N, Itoh M, Noda T, Matsuura M, et al. Inhibitory effects of mofezolac, a cyclooxygenase-1 selective inhibitor, on intestinal carcinogenesis. Carcinogenesis 2002;23:1463–6.
[3] Daikoku T, Wang D, Tranguch S, Morrow JD, Orsulic S, DuBois RN, et al. Cyclooxygenase-1 is a potent target for prevention and treatment of ovarian epithelial cancer. Cancer Res 2005;65:3735–44.
[4] Cathcart M-C, O'Byrne KJ, Reynolds JV, O'Sullivan J, Pidgeon GP. COX-derived prostanoid pathways in gastrointestinal cancer development and progression: novel targets for prevention and intervention. Biochim Biophys Acta 2012; 1825:49–63.
[5] Chandrasekharan NV, Dai H, Roos KL, Evanson NK, Tomsik J, Eltan TS, et al. COX-3, a cyclooxygenase-1 variant inhibited by acetaminophen and other analgesic/antipyretic drugs: cloning, structure and expression. Proc Natl Acad Sci U S A 2002;99:13926–31.
[6] Warner T-D, Mitchell JA. Cyclooxygenase-3 (COX-3): filling in the gaps toward a COX continuum? Proc Natl Acad Sci U S A 2002;99:13371–3.
[7] Simmons DL, Botting RM, Hla T. Cyclooxygenase isozymes: the biology of prostaglandin synthesis and inhibition. Pharmacol Rev 2004;56:387–437.
[8] Krumbail RG, Kiefer JR, Marnett LJ. Cyclooxygenase enzymes: catalysis and inhibition. Curr Opin Struct Biol 2001;11:752–60.
[9] Picot D, Loll PJ, Garavlto RM. The X-ray crystal structure of the membrane protein prostaglandin H_2 synthase-1. Nature 1994;367:243–9.
[10] Kurumbail RG, Stevens AM, Gierse JK, McDonald JJ, Stegeman RA, Pak JY, et al. Structural basis for selective inhibition of cyclooxygenase-2 by anti-inflammatory agents. Nature 1996;384:644–8.
[11] Smith WL, Urade Y, Jokobsson P-J. Enzymes of the cyclooxygenase pathways of prostanoid biosynthesis. Chem Rev 2011;111:5821–65.
[12] Vecchio AJ, Simmons DM, Malkowski MG. Structural basis of fatty acid substrate binding to cyclooxygenase-2. J Biol Chem 2010;285:22152–63.
[13] Prusakiewicz JJ, Duggan KC, Rouzer CA, Marnett L. Differential sensitivity and mechanism of inhibition of COX-2 oxygenation of arachidonic acid and 2-arachidonoylglycerol by ibuprofen and mefenamic acid. Biochemistry 2009; 48:7353–5.
[14] Dong L, Vecchio AJ, Sharma NP, Jurban BJ, Malkowski MG, Smith WL. Human cyclooxygenase-2 is a sequence homodimer that functions as a conformational heterodimer. J Biol Chem 2011;286:19035–46.
[15] Davis NM, Wallace JL. Nonsteroid anti-inflammatory drug-induced gastrointenstinal toxicity: new insights into an old problem. J Gastroenterol 1997; 32:127–33.
[16] Richy F, Bruyere O, Ethgen O, Raben da V, Bouvenot G, Audran M, et al. Time dependent risk of gastrointestinal complications induced by non-steroidal anti-inflammatory drug use: a consensus statement using a meta-analytic approach. Ann Rheum Dis 2004;766:759–66.
[17] Piazza GA, Keeton AB, Tinsley HN, Gary BD, Whitt JD, Mathew B, et al. A novel sulindac derivative that does not inhibit cyclooxygenases but potently inhibits colon tumor cell growth and induces apoptosis with antitumor activity. Cancer Prev Res 2009;2:572–80.
[18] Kakuta H, Zheng X, Oda H, Harada S, Sugimoto Y, Sasaki K, et al. Cyclooxygenase-1-selective inhibitors are attractive candidates for analgesics that do not cause gastric damage. Design and in vitro/in vivo evaluation of a benamide type cyclooxygenase-1 selective inhibitor. J Med Chem 2008;51:2400–11.
[19] Liedtke AJ, Crews BC, Daniel CM, Blobaum AL, Kingsley PJ, Ghebreselasie K, et al. Cyclooxygenase-1selective inhibitors based on the (E)-2′-Des-methyl-sulindac sulfide scaffold. J Med Chem 2012;55:2287–300.
[20] Wallace JL, Mcknight W, Reuter BK, Vegnolle N. NSAID-induced gastric damage in rats: requirement for inhibition of both cyclooxygenase 1 and 2. Gastroenterology 2000;119:706–14.
[21] de Vries EF, van Waarde A, Buursma AR, Vaalburg W. Synthesis and in vivo evaluation of F-18-desbromo-DuP-697 as a PET tracer for cyclooxygenase-2 expression. J Nucl Med 2003;44:1700–6.
[22] McCarthy TJ, Sheriff AU, Graneto MJ, Talley JJ, Welch MJ. Radiosynthesis, in vitro validation, and in vivo evaluation of ^{18}F-labeled COX-1 and COX-2 inhibitors. J Nucl Med 2002;43:117–24.
[23] Prabhakaran J, Underwood MD, Parsey RV, Arango V, Majo VJ, Simpson NR, et al. Synthesis and in vivo evaluation of [F-18]-4-[5-(4-methylphenyl)-3-(trifluoromethyl)-1H-pyrazol-1-yl]benzenesulfonamide as a PET imaging probe for COX-2 expression. Bioorg Med Chem 2007;15:1802–7.

Please cite this article in press as: Huang H-L, et al., [^{123}I]Iodooctyl fenbufen amide as a SPECT tracer for imaging tumors that over-express COX enzymes, Biomaterials (2013), http://dx.doi.org/10.1016/j.biomaterials.2013.01.050

[24] Wuest F, Hohne A, Metz P. Synthesis of F-18-labelled cyclooxygenase-2 (COX-2) inhibitors via Stille reaction with 4-[F-18]fluoroiodobenzene as radiotracers for positron emission tomography (PET). Org Biomol Chem 2005;3:503–7.
[25] Majo VJ, Prabhakaran J, Simpson NR, Van Heertum RL, Mann JJ, Kumar JS. A general method for the synthesis of aryl [C-11]methylsulfones: potential PET probes for imaging cyclooxygenase-2 expression. Bioorg Med Chem Lett 2005;15:4268–71.
[26] de Vries EF, Doorduin J, Dierckx RA, van Waarde A. Evaluation of [C-11] rofecoxib as PET tracer for cyclooxygenase 2 overexpression in rat models of inflammation. Nucl Med Biol 2008;35:35–42.
[27] Toyokuni T, Kumar JS, Walsh JC, Shapiro A, Talley JJ, Phelps ME, et al. Synthesis of 4-(5-[F-18]fluoromethyl-3-phenylisoxazol-4-yl)-benzenesulfonamide, a new [F-18]fluorinated analogue of valdecoxib, as a potential radiotracer for imaging cyclooxygenase-2 with positron emission tomography. Bioorg Med Chem Lett 2005;15:4699–702.
[28] Fujisaki Y, Kawamura K, Wang WF, Ishiwata K, Yamamoto F, Kuwano T, et al. Radiosynthesis and in vivo evaluation of C-11-labeled 1,5-diarylpyrazole derivatives for mapping cyclooxygenases. Ann Nucl Med 2005;19:617–25.
[29] Tian H, Lee Z. Synthesis of F-18-labeled cyclooxygenase-2 (COX-2) inhibitor as a potential PET imaging agent. J Label Compd Radiopharm 2006;49:583–93.
[30] Tanaka M, Fujisaki Y, Kawamura K, Ishiwata K, Qinggeletu, Yamamoto F, et al. Radiosynthesis and evaluation of C-11-labeled diaryl-substituted imidazole and indole derivatives for mapping cyclooxygenase-2. Biol Pharm Bull 2006;29:2087–94.
[31] Yang DJ, Bryant J, Chang JY, Mendez R, Oh CS, Yu DF, et al. Assessment of cyclooxygense-2 expression with Tc-99m-labeled celebrex. Anticancer Drugs 2004;15:255–63.
[32] Kabalka GW, Mereddy AR, Schuller HM. Synthesis of an iodine-123-labeled celecoxib analogue: a potential SPECT agent. J Label Compd Radiopharm 2005;48:295–300.
[33] Reitz DB, Li JJ, Norton MB, Reinhard EJ, Collins JT, Anderson GD, et al. Selective cyclooxygenase inhibitors – novel 1,2-diarylcyclopentenes are potent and orally-active cox-2 inhibitors. J Med Chem 1994;37:3878–81.
[34] Li JJ, Anderson GD, Burton EG, Cogburn JN, Collins JT, Garland DJ, et al. 1,2-Diarylcyclopentenes as selective cyclooxygenase-2 inhibitors and orally-active antiinflammatory agents. J Med Chem 1995;38:4570–8.
[35] Wuest F, Kniess T, Bergmann R, Pietzsch J. Synthesis and evaluation in vitro and in vivo of a (11)C-labeled cyclooxygenase-2 (COX-2) inhibitor. Bioorg Med Chem 2008;16:7662–70.
[36] Uddin Md J, Crews BC, Ghebreselasie K, Tantawy MN, Marnett LJ. [I-123]-celecoxib analogues as SPECT tracers of cyclooxygenase-2 in inflammation. ACS Med Chem Lett 2011;2:160–4.
[37] Lappin G, Garner RC. Big physics, small doses: the use of AMS and PET in human microdosing of development drugs. Nat Rev Drugs Discov 2003;2:233–40.
[38] Takashima-Hirano M, Shukuri M, Takashima T, Goto M, Wada Y, Watanabe Y, et al. General method for the C-11-labeling of 2-arylpropionic acids and their esters: construction of a PET tracer library for a study of biological events involved in COXs expression. Chem Eur J 2010;16:4250–8.
[39] Shukuri M, Takashima-Hirano M, Tokuda K, Takashima T, Matsumura K, Inoue O, et al. In vivo expression of cyclooxygenase-1 in activated microglia and macrophages during neuroinflammation visualized by PET with C-11-ketoprofen methyl ester. J Nucl Med 2011;52:1094–101.
[40] Chiang L-W, Pei K, Chen S-W, Huang H-L, Lin K-J, Yen T-C, et al. Combining a solution-phase derived library with in-situ cellular bioassay: prompt screening of amide-forming minilibraries using MTT assay. Chem Pharm Bullet 2009;57:714–8.
[41] Su Y-H, Chiang L-W, Jeng K-C, Huang H-L, Chen J-T, Lin W-J, et al. Solution-phase parallel synthesis and screening of anti-tumor activities from fenbufen and ethacrynic acid libraries. Bioorg Med Chem Lett 2011;21:1320–4.
[42] Lin K-I, Yang C-H, Huang C-W, Jian J-Y, Huang Y-C, Yu C-S. Synthesis and structure-activity relationships of fenbufen amide analogs. Molecules 2010;15:8796–803.
[43] Yu M, Ives D, Ramesha CS. Synthesis of prostaglandin E-2 ethanolamide from anandamide by cyclooxygenase-2. J Biol Chem 1997;272:21181–6.
[44] Kuc C, Jenkins A, Van dross RT. Arachidonoyl ethanolamide (AEA)-induced apoptosis is mediated by J-series prostaglandins and is enhanced by fatty acid amide hydrolase (FAAH) blockade. Mol Carcinog 2012;51:139–49.
[45] Husain A, Ahmad A, Alam MM, Ajmal M, Ahuja P. Fenbufen based 3-[5-(substituted aryl)-1,3,4-oxadiazol-2-yl]-1-(biphenyl-4-yl)propan-1-ones as safer antiinflammatory and analgesic agents. Eur J Med Chem 2009;44:3798–804.
[46] Tsai AL, Kulmacz RJ. Prostaglandin H synthase: resolved and unresolved mechanistic issues. Arch Biochem Biophys 2010;493:103–24.
[47] Gerhauser C, Klimo K, Heiss E, Neumann I, Gamal-Eldeen A, Knauft J, et al. Mechanism-based in vitro screening of potential cancer chemopreventive agents. Mutat Res-Fundam Mol Mech Mutagen 2003;523:163–72.
[48] Kang SS, Cuendet M, Endringer DC, Croy VL, Pezzuto JM, Lipton MA. Synthesis and biological evaluation of a library of resveratrol analogues as inhibitors of COX-1, COX-2 and NF-kappa B. Bioorg Med Chem 2009;17:1044–54.
[49] Seibert K, Zhang Y, Leahy K, Hauser S, Masferrer J, Perkins W, et al. Pharmacological and biochemical demonstration of the role of cyclooxygenase-2 in inflammation and pain. Proc Natl Acad Sci U S A 1994;91:12013–7.
[50] Brenneis C, Maier TJ, Schmidt R, Hofacker A, Zulauf L, Jakobsson PJ, et al. Inhibition of prostaglandin E2 synthesis by SC-560 is independent of cyclooxygenase 1 inhibition. Faseb J 2006;20:1352–60.
[51] Liver Cancer Study Group of Japan. Classification of primary liver cancer. 1st English ed. Tokyo: Kanehara Shuppan; 1997.
[52] Shaib Y, El-Serag HB. The epidemiology of cholangiocarcinoma. Semin Liver Dis 2004;24:115–25.
[53] Shaib YH, Davila JA, McGlynn K, El-Serag HB. Rising incidence of intrahepatic cholangiocarcinoma in the United States: a true increase? J Hepatol 2004;40:472–7.
[54] Patel T. Worldwide trends in mortality from biliary tract malignancies. BMC Cancer 2002;2:10.
[55] Chang KY, Chang JY, Yen Y. Increasing incidence of intrahepatic cholangiocarcinoma and its relationship to chronic viral hepatitis. J Natl Compr Canc Netw 2009;7:423–7.
[56] Yeh CN, Lin KJ, Hsiao IT, Yen TC, Chen TW, Jan YY, et al. Animal PET for thioacetamide-induced rat cholangiocarcinoma: a novel and reliable platform. Mol Imaging Biol 2008;10:209–16.
[57] Huang H-L, Yeh C-N, Chang K-W, Chen J, Lin K-J, Chiang L-W, et al. Synthesis and evaluation of [^{18}F]fluorobutyl ethacrynic amide: a potential PET tracer for studying glutathione transferase. Bioorg Med Chem Lett 2012;22:3998–4003.

Please cite this article in press as: Huang H-L, et al., [^{123}I]Iodooctyl fenbufen amide as a SPECT tracer for imaging tumors that over-express COX enzymes, Biomaterials (2013), http://dx.doi.org/10.1016/j.biomaterials.2013.01.050